

Article

# Active Flutter Suppression of a Wing Section in the Subsonic, Sonic and Supersonic Regimes by the $H_\infty$ Control Method

Álvaro Muñoz  and Pablo García-Fogeda \* 

Department of Aircraft and Space Vehicles, ETSIAE, Universidad Politécnica de Madrid, 28040 Madrid, Spain; alvaro.mnzm@gmail.com

\* Correspondence: pablo.garciafogeda@upm.es

**Abstract:** This paper compares various procedures for determining the optimal control law for a wing section in compressible flow. The flow regime includes subsonic, sonic and supersonic flows. For the evolution of the system in the Laplace plane, the present method makes use of the exact unsteady aerodynamic forces in this plane once the control law is established. This is a great advantage over other results previously published, where the unsteady aerodynamics in the Laplace plane are merely approximations of the curve-fitted values in the frequency domain (imaginary axis). A comparison of different control techniques like pole placement, LQR and H-infinity control demonstrates that the H-infinity controller is the optimal choice, exhibiting an H-infinity norm approximately two orders of magnitude lower than the LQR case. Furthermore, the H-infinity controller demonstrates lower pole values than those of the pole placement and LQR compensator, showing the advantage of the H-infinity controller in terms of economic efficiency.

**Keywords:** aeroservoelasticity; active flutter suppression; unsteady aerodynamics in the Laplace domain; H-infinity



**Citation:** Muñoz, A.; García-Fogeda, P. Active Flutter Suppression of a Wing Section in the Subsonic, Sonic and Supersonic Regimes by the  $H_\infty$  Control Method. *Aerospace* **2024**, *11*, 198. <https://doi.org/10.3390/aerospace11030198>

Academic Editor: Konstantinos Kontis

Received: 5 December 2023

Revised: 22 February 2024

Accepted: 27 February 2024

Published: 29 February 2024



**Copyright:** © 2024 by the authors. Licensee MDPI, Basel, Switzerland. This article is an open access article distributed under the terms and conditions of the Creative Commons Attribution (CC BY) license (<https://creativecommons.org/licenses/by/4.0/>).

## 1. Introduction

New high-aspect-ratio lightweight wings development is now one of the main targets in aviation, with the objective of reducing fuel consumption and diminishing greenhouse gas emissions. However, these advanced wings are more susceptible to aeroelastic instabilities, such as flutter or divergence. A solution to overcome such instabilities is the implementation of the active control on the wing structure, thus extending its flight envelope [1]. Active flutter suppression (AFS) has been known for some time; see, for example, [2,3]. Despite its potential, the practical implementation of AFS faces several challenges. These include the need for a robust method to compute unsteady aerodynamics valid in the Laplace domain, devising a control law that remains effective across the full compressible regime and determining an optimal control strategy capable of minimizing energy consumption.

As mentioned by Livne [4], for any AFS solution to be accepted, it must be fully understood and supported by reliable tools. Consequently, there exists a pressing need for a practical and robust AFS system suitable for integration into aircraft systems. For multi-input–output systems, AFS often requires many trial designs before achieving satisfactory results. Modern state-space control design methods seem more compatible with general multi-input–output systems, and many techniques like linear quadratic Gaussian (LQG) [5],  $H_\infty$  control [6–8] or pole and partial or complete eigenstructures assignment [9,10] have proven their validity for applications with multiple-input multiple-output systems. However, when applied to active flutter suppression, these methods suffer from the need to greatly augment the states of the model in order to express the generalized aerodynamic forces matrix in the state-space. These additional states are fictitious, unmeasurable and very sensitive to the modeling approximation inherent in the aerodynamic formulation used.

Linear Matrix Inequalities (LMIs) have proven to derive suboptimal designs for linear control problems [11]. Chiali and Gahinet [12] extended the LMI approach to multiobjective output feedback synthesis. Gahinet and Apkarian [13] used LMI and extended the concept of  $H_\infty$  controllers replacing the Riccati equations with Riccati inequalities to parameterize the suboptimal  $H_\infty$  controllers, including reduced-order variants.

For high-aspect-ratio wings, like the ones that are within the objective of this work, strip theory is a very valuable procedure to determine their stability and control. To apply this theory, a well-established and validated airfoil section method is required. Among others, some recent publications like Darabseh et al. [14] and Micheli [15] have considered, for an airfoil section in incompressible flow, the active flutter suppression by a linear quadratic Gaussian optimal control [14] and the influence of the actuator saturation in [15]. In this study, the compressibility effects on the unsteady aerodynamic forces will be taken into account for a wing section with three degrees of freedom. The aerodynamics fully valid in the Laplace domain presented in [16] will be used, and different procedures to determine the optimal control law will be investigated. It will be shown that the  $H_\infty$  controllers provide the best result in terms of stability for all the cases presented.

The paper's organization is as follows: Section 2 presents the equations of motion for the state-space model; in Section 3, a brief resume on the development of the standard compensator for the system stabilization is given; Section 4 introduces the  $H_\infty$  controller and discusses its internal stability; Section 5 presents the results obtained in the full Mach number regime; and Section 6 offers the concluding remarks for this work.

## 2. Equations of Motion and State-Space Modelization

The active control of a three degrees of freedom (dof) wing section (Figure 1) is considered. The control of the system is performed through the control surface (variable  $u = \delta$ ). The dynamic equation of the system in the Laplace domain, as derived in Equations 2.1 and 2.21 of Edward's work [17], is

$$\left( M_s p^2 + B_s p + K_s \right) x_q = \frac{\eta}{2} \left( \frac{U}{b} \right)^2 Q \left( \frac{pb}{U}, M_\infty \right) x_q + Gu \quad (1)$$

where  $\eta = \frac{1}{\pi\mu}$ ,  $\mu$  is the nondimensional mass ratio and  $\{x_q\} = [\frac{h}{b} \quad \alpha \quad \delta]^T$  are the structural degrees of freedom; the structural inertia, damping and rigidity matrices are after nondimensionalization, given as

$$M_s = \begin{bmatrix} 1 & x_\alpha & x_\delta \\ x_\alpha & r_\alpha^2 & r_\delta^2 + \Lambda_{31} x_\delta \\ x_\delta & r_\delta^2 + \Lambda_{31} x_\delta & r_\delta^2 \end{bmatrix}, B_s = \begin{bmatrix} 0 & 0 & 0 \\ 0 & 0 & 0 \\ 0 & 0 & 2r_\delta^2 \omega_\delta \zeta_\delta \end{bmatrix}, K_s = \begin{bmatrix} \omega_h^2 & 0 & 0 \\ 0 & r_{alpha}^2 \omega_\alpha^2 & 0 \\ 0 & 0 & r_\delta^2 \omega_\delta^2 \end{bmatrix} \quad (2)$$

where  $\Lambda_{31} = \Lambda_3 - \Lambda_1$  and  $G$  is the gain matrix given by

$$G = \begin{bmatrix} 0 \\ 0 \\ r_\delta^2 \omega_\delta^2 \end{bmatrix}, \quad (3)$$

$Q(\frac{pb}{U}, M_\infty)$  accounts for the unsteady aerodynamic loads matrix obtained in the Laplace plane, and  $u$  is the external moment applied to the control surface. In this work, the aerodynamic forces are valid in the complete Laplace plane since they are not determined by an approximation or curve fitting of the unsteady aerodynamic forces in the frequency domain. This is a big advantage of the proposed method since, as pointed out by several investigators [18], the curve fit approximations may have questionable applicability out of the imaginary axis of the Laplace plane. In Ref. [16], a detailed description of how these aerodynamic forces have been calculated in the subsonic, transonic and supersonic linear flows can be found. For the subsonic flow, a collocation method is developed; for the flow at the sonic Mach number, the solution of Rott [19] has been generalized to the Laplace

domain; and for supersonic flows, the solution of Garrick applied to the Laplace plane by [17] has been used. The generalized force matrix can then be expressed in a uniform manner as a function of the nondimensional Laplace variable  $s = \frac{pb}{U}$  and of the Mach number as  $[Q_{ij}(s, M_\infty)]$ , where  $i, j$  is the state for  $\frac{h}{c/2}$ ,  $\alpha$  and  $\delta$ .

Then, Equation (1) in the nondimensional Laplace variable  $s$  can be expressed as

$$\left( M_s \left( \frac{U}{b} \right)^2 s^2 + B_s \left( \frac{U}{b} \right) s + K_s - \frac{\eta}{2} \left( \frac{U}{b} \right)^2 Q(s, M_\infty) \right) x_q = Gu \tag{4}$$

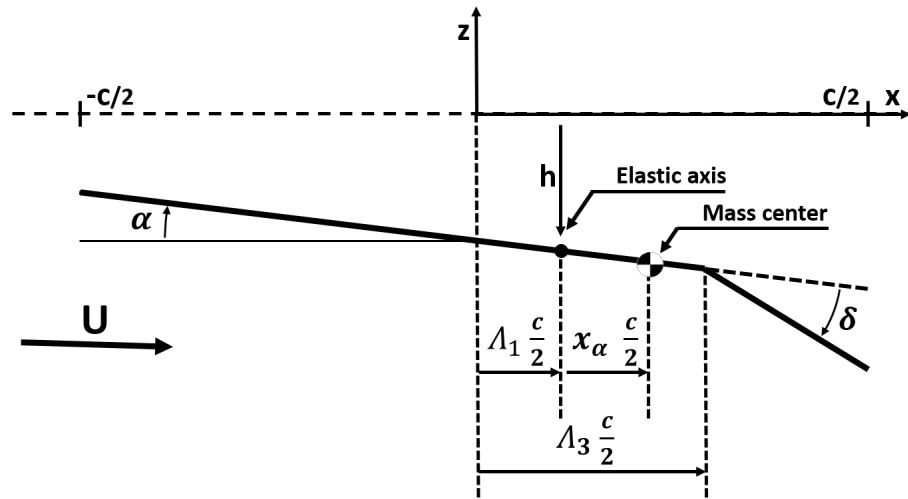


**Figure 1.** Diagram of a typical airfoil section with three degrees of freedom: plunging, pitching and trailing-edge control surface.

In order to manipulate the system and to obtain an adequate control law, the system's equations of motion must be transformed to the state-space. For the control law evaluation, a Rational Function Approximation (RFA) methodology will be employed, following Roger's model [20]. It must be noted that the use of RFAs introduces inherent inaccuracies in the model since the data fitting may not be exact. Although RFA has been widely used for control law evaluations, recently, a new method based on tangential interpolation [21] has also proved to be a valid approach instead of the RFA. In this work, however, the RFA will only be used to compute the control law, and the exact dynamic equation will be applied when presenting the resultant behavior in a closed-loop configuration, with this being one of the main advantages of the proposed method.

Roger's approximation contains a number of common lags, representing the aerodynamic lag of the system. Its usual expression is presented by Karpel [3] as

$$Q(s, M_\infty) = -A_0 - A_1s - A_2s^2 - \sum_{j=3}^N \frac{A_j s}{s + \gamma_{j-2}} \tag{5}$$

As the model's order grows linearly with the number of lags, it is not advisable to select a high number of lag states. Typically,  $N = 6$  is enough for most applications, as suggested by Karpel. When represented in matrix form, this RFA can be conveniently expressed as

$$Q(s, M_\infty) = -A_0 - A_1s - A_2s^2 - D(sI - R)^{-1}Es \tag{6}$$

where  $R$  contains the lags of the system (common for all the degrees of freedom) and  $D$  acts as a summation matrix.

To determine the matrices  $A_0$ ,  $A_1$ ,  $A_2$  and  $E$ , an adequate number of generalized aerodynamic force matrices to fit the model must be provided. A conventional approach involves computing these loads under the assumption of simple harmonic oscillations, i.e., pure imaginary reduced frequencies. However, by incorporating data from across the Laplace plane, the model is expected to increase its accuracy far from the imaginary axis. These aerodynamic loads serve as the foundation for fitting the model through the use of a least squares method [22]. Additionally, the incorporation of Lagrange multipliers enables the imposition of steady load values, with the flexibility to introduce additional constraints if necessary, such as the frequency derivative of the loads in the proximity to  $s = 0$ . This condition can only be applied in the subsonic regime since for  $M_\infty = 1$ , there exists a singularity in the aerodynamic loads for  $s = 0$ ; see also [19] for the case of  $k = 0$  for harmonic oscillations.

In order to validate the RFA, the approximate loads are compared with the exact ones in Figure 2. The loads are computed along three branches in the form  $s = |s| \exp(i\theta)$ . For the fitting of the RFA,  $N = 6$  is used, and values of the complex Laplace variable  $s$  are computed within the region of interest. It is noteworthy that the fitting process is performed based on the loads obtained in the full Laplace plane and not only along the imaginary axis. The results reveal a close match between the loads from the RFA and the exact results. However, the accuracy of the approximation significantly depends on the selected values of  $s$  used when moving away from the imaginary axis.

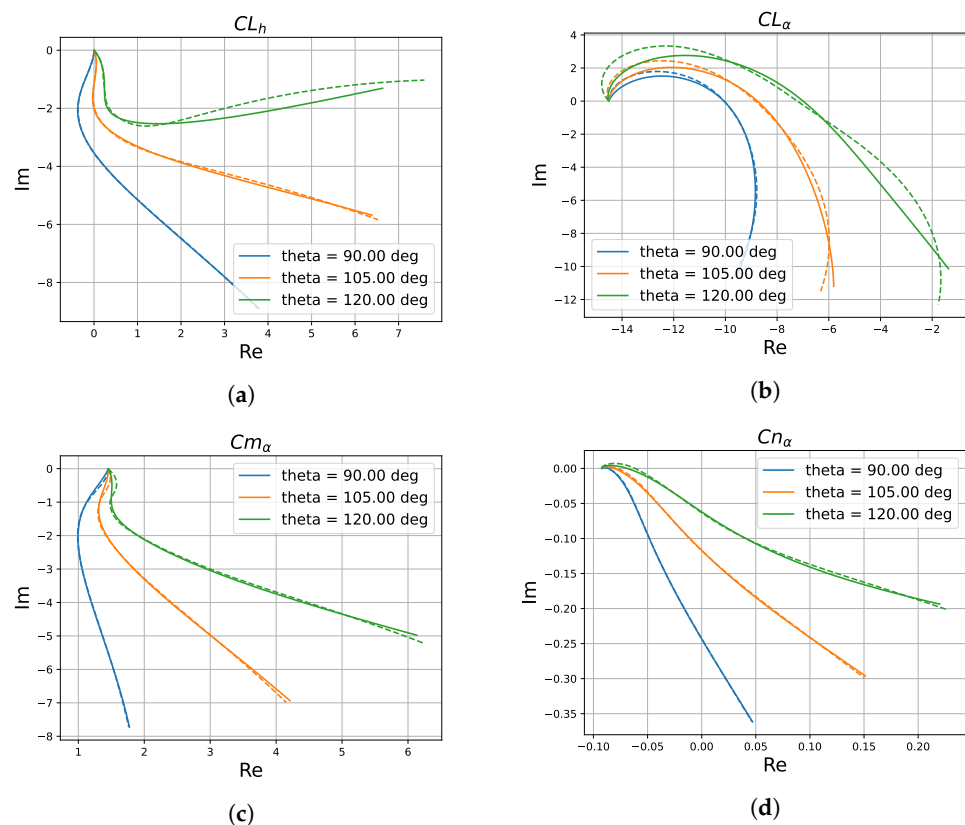


**Figure 2.** Unsteady aerodynamic loads of an airfoil with three degrees of freedom, with  $\Lambda_1 = -0.4$  and  $\Lambda_3 = 0.6$ , in subsonic compressible flow at  $M_\infty = 0.5$ . Exact loads are presented with a continuous line, while results from the RFA are plotted with a dashed line. (a) Lift coefficient for a plunging airfoil. (b) Lift coefficient for an oscillating airfoil. (c) Pitching moment coefficient for an oscillating airfoil. (d) Hinge moment coefficient for an oscillating airfoil.

Once the coefficients of the RFA are obtained, the equations of the augmented aerodynamic states  $x_a$ , which are based on the lags within the RFA, can be expressed as a function of the system states  $x_q$  through a linear relation with the  $s$  variable. The aerodynamic states can then be defined as follows:

$$x_a = (sI - R)^{-1} E s x_q \quad (7)$$

where  $R$  and  $D$  were obtained directly from Equation (6), with  $s x_q$  being the derivatives of the system states.

Subsequently, the aerodynamic loads can be expressed as

$$Q(s, M_\infty) x_q = \left( -A_0 - A_1 s - A_2 s^2 \right) x_q - D x_a \quad (8)$$

By incorporating these aerodynamic loads into the dynamic system and reorganizing the matrices, the resulting state equation takes the form

$$\left[ M_t s^2 + B_t s + K_t \right] x_q + D_t x_a = G u \quad (9)$$

where

$$M_t = \left( M_s + \frac{\eta}{2} A_2 \right) \left( \frac{U}{b} \right)^2, \quad B_t = \left( B_s + \frac{\eta}{2} \left( \frac{U}{b} \right) A_1 \right) \left( \frac{U}{b} \right)$$

$$K_t = K_s + \frac{\eta}{2} \left( \frac{U}{b} \right)^2 A_0, \quad D_t = \frac{\eta}{2} \left( \frac{U}{b} \right)^2 D$$

Here, the matrices  $M_t$ ,  $B_t$ ,  $K_t$  and  $D_t$  are defined in terms of airspeed and Mach number, considering that the RFA has also been computed for the same Mach number,  $M_\infty$ . These matrices collectively represent the system dynamics for a given operating condition.

Gathering these equations in a matricial form, the resulting state-space model possesses a total of  $N_{dof} \times N$  states (with  $N_{dof}$  typically being three), and it is expressed as

$$s \begin{Bmatrix} x_q \\ s x_q \\ x_a \end{Bmatrix} = \begin{bmatrix} 0 & I & 0 \\ -M_t^{-1} K_t & -M_t^{-1} B_t & -M_t^{-1} D_t \\ 0 & E & R \end{bmatrix} \begin{Bmatrix} x_q \\ s x_q \\ x_a \end{Bmatrix} + \begin{bmatrix} 0 \\ M_t^{-1} G \\ 0 \end{bmatrix} u \quad (10)$$

The expanded states, together with the initial vector  $x_q$  and its nondimensional derivatives, form a new state vector,  $x$ . The equation determining the internal dynamics of the state-space system is then expressed as

$$s x = A x + B u \quad (11)$$

This time-invariant system is validated by comparing the root locus of a typical airfoil obtained by using the p-method solution of Equation (4) with the poles of the state-space model and the RFA applied solution to Equation (10), as illustrated in Figure 3. The specific airfoil parameters are detailed in Table 1.

**Table 1.** Three DOF section parameters for a wing section in compressible flow, extracted from Table III-3 of Edward's thesis [17].

$\Lambda_1 = -0.4$	$\omega_h = 50$ Hz	$x_\alpha = 0.2$	$x_\delta = 0.0125$
$\Lambda_3 = 0.6$	$\omega_\alpha = 100$ Hz	$r_\alpha^2 = 0.25$	$r_\delta^2 = 0.00625$
$\mu = 40$	$\omega_\beta = 300$ Hz		$\zeta_\delta = 0$

In this context,  $x_\alpha$  represents the nondimensional distance from the center of mass to the elastic axis,  $r_\alpha^2$  represents the nondimensional radius of gyration of the airfoil,  $x_\delta$  represents the nondimensional distance from the center of mass of the control surface to the

hinge axis and  $r_\delta^2$  stands for the nondimensional radius of gyration of the control surface. Additionally,  $\Lambda_1$  corresponds to the nondimensional location of the elastic axis,  $\Lambda_3$  to the nondimensional separation between the elastic axis and the hinge axis of the control surface and  $\zeta_\delta$  denotes the nondimensional damping coefficient of the control surface mode.

In Figure 3, it can be observed that for the subsonic regime at  $M_\infty = 0.5$ , our state-space analysis closely matches the results derived from the exact solution, expressed in the Laplace plane (Equation (4)) obtained previously at [16]. However, for higher Mach numbers, we notice a mismatch mainly in the aileron mode. Although the RFA used here considers values out of the imaginary axis, some differences with respect to the exact p-method are still observed. If the fitting is made by taking only points along the imaginary axis, a larger difference would occur with respect to the exact solution given by the p-method. Therefore, despite these small discrepancies, we will proceed with our calculations as the plunging and torsion modes align well with our model.

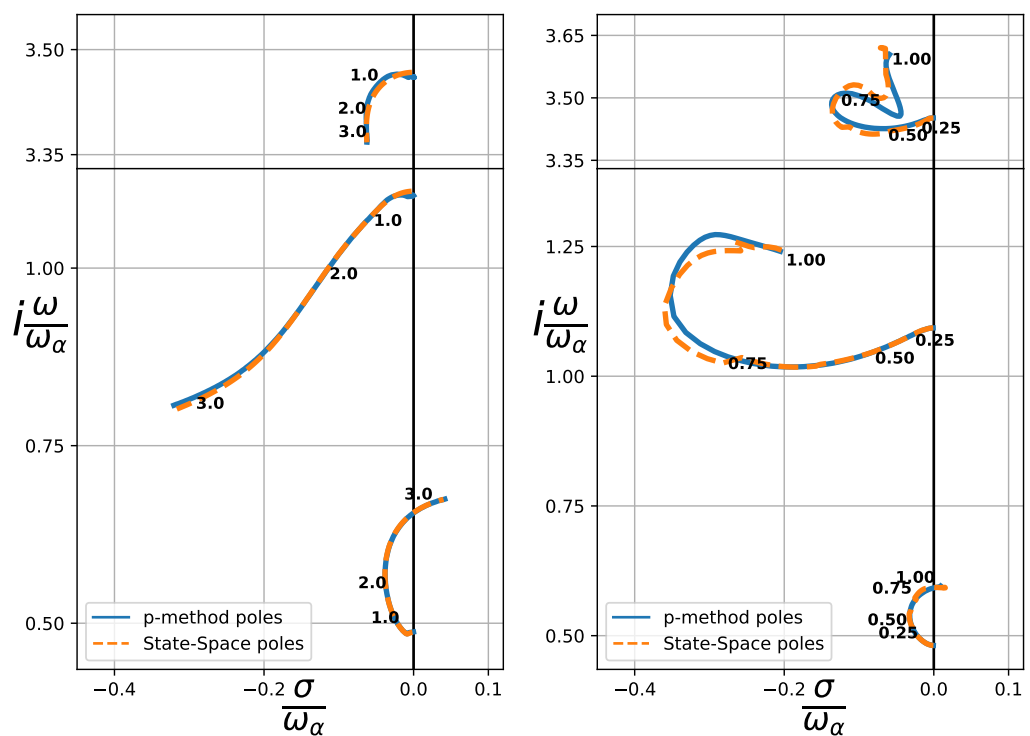


**Figure 3.** Root locus comparison of the p-method poles and the state-space system poles for a 3 dof airfoil. Left figure assumes constant Mach  $M_\infty = 0.5$  (for increasing  $U/b\omega_\alpha$ , indicated in the figure), while right one considers variable Mach number (indicated in the figure, with  $a_\infty = 300$  m/s).

### 3. Standard Compensator

In order to stabilize the system, the implementation of a control law based on the state-space system is required. Various control strategies have been studied either theoretically or implemented in active flutter suppression, including proportional–integral–derivative control (PID), pole placement, the Linear Quadratic Regulator (LQR) method and Kalman filters [23], among other options. In this work, the first approach will be to study the stabilization of the system by the use of pole placement and the LQR method.

The control loop can be split into two essential parts, each serving a specific role in the overall control strategy. First, we have the feedback gain matrix, known as  $K$ , which is responsible for generating the control input  $u$ . This input relies on the estimated full state vector,  $\hat{x}$ , representing the internal states. These states are estimated by using a linear observer, which uses the system’s output vector  $y$  to track the system evolution over time. The separation principle states that the regulator and the estimator can be implemented

separately, simplifying the control system design. The implementation of an observer together with a regulator is often referred to as a compensator.

In this section, a control law will be derived based on the previously presented state-space system. First, the state-space system will be completed. Subsequently, an examination of the system's controllability and observability will be undertaken. Then, an observer and a regulator will be separately obtained. Finally, the effectiveness and efficiency of the resulting control law will be assessed.

### 3.1. Completion of the State-Space Model

The state-space system presented in Equation (10) must be completed since it only has information on the states of the system and its inputs. To accomplish this, the output matrix  $C$  is defined here. In our particular system, the moment applied to the control surface cannot be measured directly, so the direct transmission matrix of the system,  $D$ , is set to zero. Hence, the output equation is

$$y = Cx + Du = Cx \quad (12)$$

As established earlier, the system's states include both physical and aerodynamic states. Only the physical states ( $h, \alpha, \delta$  and its derivatives) can be measured directly; therefore, the output matrix is defined as

$$C = \begin{bmatrix} [I]_{6 \times 6} & [0]_{6 \times (N-2)} \end{bmatrix} \quad (13)$$

In this case, it is assumed that we are measuring all the physical states of the system. In practice, one should include here only the states that can be measured by using the available sensor configuration.

Gathering the state-space matrices, a linear time-invariant system is obtained, represented through the standard formulation

$$\begin{aligned} \dot{x} &= Ax + Bu \\ y &= Cx \end{aligned} \quad (14)$$

### 3.2. Controllability Matrix

Given the high number of states ( $6 + 3(N - 2)$ ) compared to the number of control inputs (1), it is possible that the system is not fully controllable. The controllability matrix [24] is defined as

$$P = [B \quad AB \quad A^2B \quad \dots \quad A^{n-1}B] \quad (15)$$

with  $n$  being the rank of matrix  $A$ .

By definition, a system is considered controllable if the rank of its controllability matrix matches the rank of the system itself. As expected, the investigated airfoils are uncontrollable. Nevertheless, an uncontrollable system may still be stabilizable. This can be achieved by breaking down the system into controllable and uncontrollable subsystems and, provided that the uncontrollable one is stable, a control law can be derived that stabilizes the full system. The decomposition will be carried out hereafter.

### 3.3. Decomposition into Controllable and Uncontrollable Subsystems

Let  $P$  be the controllability matrix of the system and assume  $\text{rank}(P) \equiv q < n$ . An invertible matrix  $T \in \mathbb{R}^{n \times n}$  can be found that transform the system into its echelon form:

$$TP \equiv \tilde{P} = \begin{bmatrix} \tilde{P}_1 \\ 0 \end{bmatrix} \quad (16)$$

Let  $\tilde{x} = Tx = [\tilde{x}_c \ \tilde{x}_u]^T$  be the new states, with  $\tilde{x}_c$  and  $\tilde{x}_u$  being the controllable and uncontrollable states. The state-space system then becomes

$$\begin{aligned} s\tilde{x} &= TAT^{-1}\tilde{x} + TBu = \tilde{A}\tilde{x} + \tilde{B}u \\ y &= CT^{-1}\tilde{x} = \tilde{C}\tilde{x} \end{aligned} \quad (17)$$

The resulting matrices  $\tilde{A}$ ,  $\tilde{B}$  have the form

$$\tilde{A} = \begin{bmatrix} A_c & A_{12} \\ 0 & A_u \end{bmatrix}, \quad \tilde{B} = \begin{bmatrix} B_c \\ 0 \end{bmatrix} \quad (18)$$

The system  $A_c$  can be controlled independently from  $A_u$  since

$$\mathbf{eig}(A) = \mathbf{eig}(A_c) \cup \mathbf{eig}(A_u) \quad (19)$$

Now, a control law can be developed that feeds the controllable states to the input, following the expression  $u = K_c\tilde{x}_c$ . The control matrix  $K_c$  can be obtained for the subsystem  $(A_c, B_c)$  via pole placement or any other method. To apply the resulting matrix to the original system, the similarity transformation is reversed:

$$u = Kx = \tilde{K}Tx = [K_c \ 0]Tx \quad (20)$$

### 3.4. Regulator Implementation

In order to achieve the desired behavior of the system, the pole-placement method is introduced. This technique is based on the canonical transformation of the system, with its algorithm for MIMO systems presented by Nguyen [25,26].

The application of this algorithm yields a feedback matrix tailored to the controllable subsystem. Following Equation (20), the resulting control law takes the full state as an input:

$$u = Kx \quad (21)$$

However, conventional pole placement results in numerical instabilities during the algorithm implementation. While such instabilities may not significantly impact systems with a limited number of states, due to the large number of aerodynamic states created in this model, an exact placement of the poles cannot be achieved. Valášek and Olgac [27] presented a modified approach that minimizes these errors.

The primary challenge in this method lies in the arbitrary selection of the target poles, which often overlooks the significance of the controller's own poles. The consequences of this choice will be exposed later.

### 3.5. Linear Observer Implementation

A linear observer, often referred to as a state observer or estimator, mimics the behavior of the system by using available sensor measurements and knowledge of the system's dynamics. Since the model is a representation of reality, it will not be exact due to nonlinearities in the original model or to modeling inaccuracies. To amend these differences, the observer is corrected with the available system output. The state equation governing the observer's behavior is as follows:

$$\begin{aligned} s\hat{x} &= A\hat{x} + Bu + L(y - \hat{y}) \\ \hat{y} &= C\hat{x} \end{aligned} \quad (22)$$

with  $L$  being the observer gain matrix.

Since the estimated output is available from the second equation, the system can be expressed as

$$s\hat{x} = (A - LC)\hat{x} + Bu + Ly \quad (23)$$

The observer’s dynamics are given by the eigenvalues of the matrix  $A - LC$ . The observer matrix can then be obtained by pole placement or other methods in a similar manner to the regulator gain, replacing  $A$  and  $B$  with  $A^T$  and  $C^T$ . It is essential that the observer’s poles are positioned significantly distant from those of the regulator so the dynamics of the estimated states are faster than those of the regulator. A common practice involves placing the observer poles 10 times farther than those of the regulator.

In this particular case, the matrix  $L$  will be computed by the use of a Linear Quadratic Regulator (LQR). The primary objective of the LQR is to determine the adequate control inputs that minimize a quadratic cost function. This cost function typically includes terms related to the state of the system and the control input. Consequently, the primary challenge is to find an equilibrium between control effort and performance trade-offs.

### 3.6. Closed-Loop Dynamics

Once the observer gain matrix  $L$  and the regulator matrix  $K$  have been determined, the dynamics of the state-space model are completed, and a control law that ensures system stability can be derived.

Mapping the regulator inputs to the estimated state,  $u = K\hat{x}$ , and incorporating the feedback gain into Equation (23) leads to the following equation:

$$s\hat{x} = (A + BK - LC)\hat{x} + Ly \tag{24}$$

where  $y = Cx$  represents information obtained from the original plant. Combining the observer dynamics with the primary state-space model, an extended representation of the state-space model governing the closed-loop system is obtained and can be expressed as

$$\begin{Bmatrix} sx \\ s\hat{x} \end{Bmatrix} = \begin{bmatrix} A & BK \\ LC & A + BK - LC \end{bmatrix} \begin{Bmatrix} x \\ \hat{x} \end{Bmatrix} \tag{25}$$

The controller can now be derived from this extended system. Based on Equation (24), the control law is given as the transfer function:

$$u = K(sI - A + BK - LC)^{-1}Ly = K_{Comp}y \tag{26}$$

This is the control law that stabilizes the state-space model. It relies only on measurable outputs as well as the system’s reduced Laplace variable. Its analysis in the Laplace domain and its practical implementation for an airfoil system can be carried out following the schematic block diagram depicted in Figure 4.

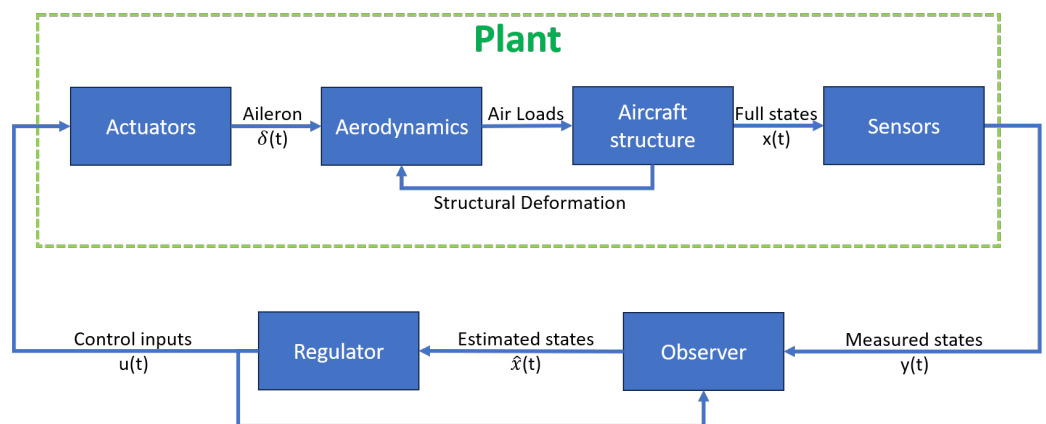


Figure 4. Block diagram of the compensator control system, consisting of a regulator and an observer.

### 3.7. Specific Control Law and Results

To proceed with the actual implementation of the control law, the parameters for the pole placement and the LQR observer must be configured. To ensure adequate system stability, a stability margin is defined to prevent the poles from approaching the imaginary axis too closely. The stable poles in the closed loop are positioned at the same locations as the open-loop branches, while those on the unstable branches are adjusted to maintain the specified stability margin. For the weight and cost matrices of the LQR controller, identity matrices are selected. For improved performance, the results can be tuned with these matrices.

To circumvent the potential inaccuracies arising from the aerodynamic model approximation, the p-method is employed to compute the pole locations. The control law has been computed based on the extended system, as illustrated in Equation (25). However, to make it applicable to the original model, it must be incorporated into Equation (4). Considering that the control law relies on the original states  $x_q$  and their derivatives, the following matrix is included in the feedback gain:

$$y = \begin{bmatrix} I \\ sI \end{bmatrix} x_q \tag{27}$$

Consequently, the dynamic equation for the system including the control law takes the form

$$\left[ M_s \left( \frac{U}{b} \right)^2 s^2 + B_s \left( \frac{U}{b} \right) s + K_s - \frac{\eta}{2} \left( \frac{U}{b} \right)^2 Q(s) - GK_{Comp}(s) \begin{bmatrix} I \\ sI \end{bmatrix} \right] x_q = 0 \tag{28}$$

with the feedback matrix defined as

$$K_{Comp}(s) = K(sI - A + BK - LC)^{-1}L \tag{29}$$

where the  $Q(s, M_\infty)$  matrix is the exact form of the aerodynamic solution without further approximation. Figure 5 shows the analysis for the root locus of the closed-loop system for the airfoil parameters given in Table 1. The control law is activated when an open-loop pole approaches the stability margin, effectively maintaining system stability for every airspeed. The originally unstable branch remains in the left plane, maintaining a stability margin from the imaginary axis. Furthermore, the system's branches remain continuous, ensuring the smooth operation of the control law across all velocities.

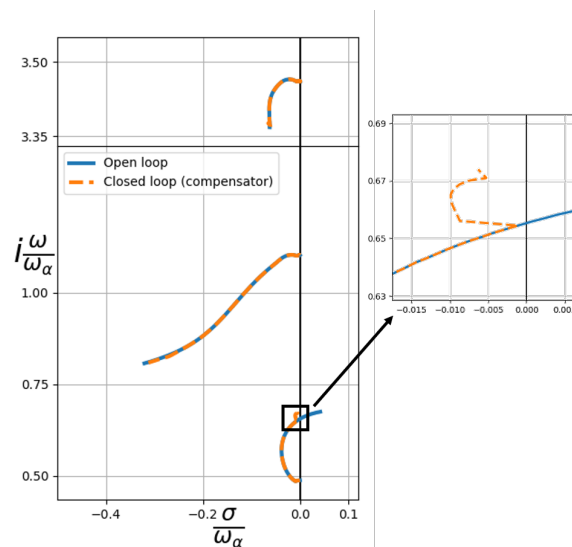


**Figure 5.** Root locus plot of a 3 dof airfoil for  $M_\infty = 0.5$  in closed loop. The control law has been obtained by the use of a compensator.

Figure 6 shows the same results, focusing on the rest of the poles from the state-space system. As anticipated, new branches emerge in the left plane, relating to the compensator poles, whose characteristics are directly influenced by the chosen control law parameters. This inherent dependence on parameter selection highlights a key limitation of this approach, as the resulting system dynamics are arbitrarily arranged by these choices.

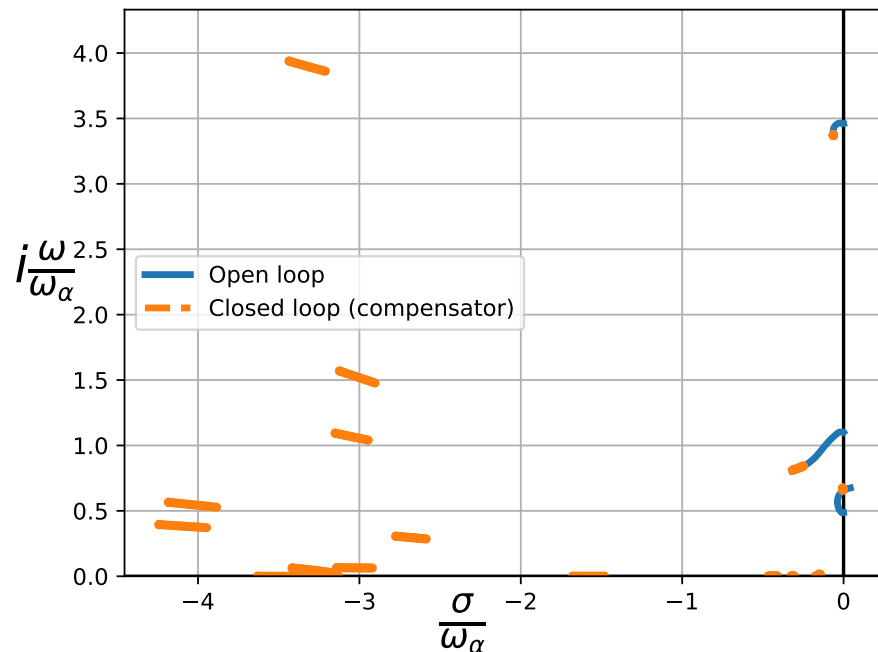


**Figure 6.** Root locus plot of the 3 dof airfoil with  $H_\infty$  controller for  $M_\infty = 0.5$ , including new branches. These poles are associated with the controller dynamics.

#### 4. $H_\infty$ H-Infinity Controller

In the preceding section, the controller derived exhibited a degree of arbitrariness due to the influence of the chosen weighting matrices within the Linear Quadratic Regulator (LQR) framework, as well as the arbitrary location of the poles. This section aims to procure an optimal controller to overcome these issues.

For this purpose, it is imperative to establish a clear definition of optimality. The primary objective herein is to formulate a controller that accomplishes system stabilization while minimizing energy consumption. Additionally, the optimal controller should demonstrate efficiency across a broad spectrum of frequencies, obviating the need for frequency-specific tuning. With these objectives in mind, the  $H_\infty$  norm of a system is introduced here.

The  $H_\infty$  (H-infinity) norm is a fundamental concept in control theory and signal processing. It serves as a critical measure of the frequency-domain performance of a system, offering insights into its robustness and stability characteristics. The  $H_\infty$  norm quantifies the maximum gain from a given input to the system's output across all frequencies, making it a powerful tool for assessing a system's susceptibility to external disturbances and uncertainties. In essence, it provides a means to evaluate the worst-case behavior of a system, which is essential for designing robust control systems and ensuring that they perform reliably under a variety of real-world conditions. Moreover,  $H_\infty$  control does not require a precise model of the system. It can accommodate modeling errors and uncertainties, making it suitable for real-world systems where accurate modeling can be challenging.

In the upcoming section, we commence by exploring the computation of the  $H_\infty$  norm. We then shift our focus to the aggregate plant, where we consider a multidimensional system encompassing various inputs and outputs, emphasizing the minimization of the  $H_\infty$  norm for regulated outputs. Next, we investigate suboptimal  $H_\infty$  controller design,

highlighting an iterative approach and the advantages of closed-form solutions. Finally, we address the issue of strong stabilization, ensuring controller stability in the presence of various factors, and present a methodology for achieving internal stability. Together, these sections provide a comprehensive overview of the application of  $H_\infty$  control to flutter alleviation systems, emphasizing the pursuit of optimal system performance while maintaining stability and reliability. Applications of this method for AFS can also be found in the work of Waitman and Marcos [28].

#### 4.1. Computation of the $H_\infty$ Norm

As has been stated, the  $H_\infty$  norm measures the worst-case behavior of a system. This assessment is achieved through the computation of the maximum singular value, denoted as  $\sigma_{\max}$ , across the entire frequency domain for a given transfer function,  $G(j\omega)$ . Consequently, the  $H_\infty$  norm is formally expressed as

$$\|G\|_\infty := \sup_{\omega} \sigma_{\max}[G(j\omega)] \quad (30)$$

Traditionally, this computation would include a Bode plot, in which the maximum response of the system would be obtained. However, Boyd, Balakrishnan and Kabamba [11] introduced an algorithmic approach for the expedient numerical estimation of the  $H_\infty$  norm. The fundamental steps of this algorithm are as follows:

1. Select an initial guess for the value for the norm of the system,  $\gamma$ .
2. Define the Hamiltonian matrix

$$H := \begin{bmatrix} A - BR^{-1}D^TC & -\gamma BR^{-1}B^T \\ \gamma C^TS^{-1}C & -A^T + C^TDR^{-1}B^T \end{bmatrix} \quad (31)$$

where  $R = (D^TD - \gamma^2I)$ ;  $S = (DD^T - \gamma^2I)$ ; and  $A, B, C$  and  $D$  are the state-space plant matrices.

3. Check if  $H$  has no eigenvalues on the imaginary axis. If so, then  $\|G\|_\infty < \gamma$ , and  $\gamma$  is subsequently decreased. Else, increase  $\gamma$ .
4. Repeat. The calculations finish when the solution converges to  $\|G\|_\infty = \gamma$ .

This method enables a more systematic and mathematically rigorous approach, reducing the reliance on graphical techniques and facilitating the optimization of systems that demand stringent performance criteria.

#### 4.2. Aggregate Plant

The  $H_\infty$  control method considers not only the closed-loop system's stability but also aims to minimize the control effort and estimation errors. Hence, the system input and outputs must be expanded to account for these variables.

For this purpose, the system is represented as a nine-matrices system, resulting in the creation of an aggregate plant with an augmented set of inputs and outputs. The expanded plant includes the following categorizations for inputs and outputs:

- Exogenous inputs  $w$ : unmodelled dynamics, sensor noise and tracking signal.
- Actuator inputs  $u$ : effect of actuators.
- Regulated outputs  $z$ : states to be minimized.
- Sensed outputs  $y$ : states that can be measured.

The dynamic equations governing the relationships among these variables are expressed as

$$\begin{aligned} sx &= Ax + B_1w + B_2u \\ z &= C_1x + D_{11}w + D_{12}u \\ y &= C_2x + D_{21}w + D_{22}u \end{aligned} \quad (32)$$

Since the objective is to minimize the effect of the exogenous inputs on the regulated outputs, the exogenous inputs must include not only potential noise and inaccuracies but also account for actuator inputs. In the context of our airfoil system, the aggregate plant, when realized in its nine-matrices representation, takes the form

$$\left[ \begin{array}{c|cc} A & B_1 & B_2 \\ \hline C_1 & D_{11} & D_{12} \\ C_2 & D_{21} & D_{22} \end{array} \right] = \left[ \begin{array}{c|cc} A & [B \ 0] & B \\ \hline [C] & 0 & [0] \\ 0 & [0 \ I] & 0 \end{array} \right] \quad (33)$$

The stabilization of the aggregate plant is achieved through the incorporation of a feedback loop from the sensed outputs to the actuator inputs. In the closed-loop configuration, the primary objective of this section is to minimize the  $H_\infty$  norm of the transfer function from exogenous inputs to regulated outputs, denoted as  $\|T_{zw}\|_\infty$ .

#### 4.3. Suboptimal $H_\infty$ Controller

Various methodologies for computing an  $H_\infty$  controller are available within the control theory domain. Notably, Gahinet and Apkarian [13] presented a method for obtaining an optimal  $H_\infty$  controller with the introduction of Linear Matrix Inequalities (LMIs). This optimization framework relies on Semidefinite Programming (SDP) and is solved through the utilization of convex optimization and Interior-Point optimization algorithms [29,30]. Nevertheless, the original method lacks the flexibility to incorporate specific constraints or limitations. Addressing this limitation, Chilali and Gahinet [12] included the use of pole placement constraints, which can be employed, for instance, to restrict the velocity of the resultant controller. Furthermore, Scherer, Gahinet and Chilali [31] expanded the method by enabling the incorporation of multiobjective output-feedback optimization.

However, the direct optimization approach using LMIs is considered less suitable for its use in this work. Firstly, the resulting controller is not guaranteed to possess internal stability, which is a crucial attribute for controller performance. Secondly, the computation of suboptimal  $H_\infty$  controllers presents a closed-form solution, which renders it a more time-efficient strategy. Consequently, in this case, it is more advantageous to first derive suboptimal  $H_\infty$  controllers and subsequently search for the optimal controller.

The objective of suboptimal  $H_\infty$  controllers will be to find all admissible controllers  $K$  such that  $\|T_{zw}\|_\infty < \gamma$ , given an arbitrary scalar  $\gamma$ . Doyle et al. [32] present a method to compute this controller based on the solution to two Algebraic Riccati Equations (AREs). The algorithm is presented hereafter.

For a given  $\gamma$ , define the following Hamiltonian matrices:

$$H_\infty = \begin{bmatrix} A & \gamma^{-2}B_1B_2^T - B_2B_2^T \\ -C_1^TC_1 & -A^T \end{bmatrix}, \quad J_\infty = \begin{bmatrix} A^T & \gamma^{-2}C_1^TC_1 - C_2^TC_2 \\ -B_1B_1^T & -A \end{bmatrix} \quad (34)$$

An admissible controller such that  $\|T_{zw}\|_\infty < \gamma$  exists if and only if the following conditions hold:

- i  $H_\infty \in \text{dom}(\text{Ric})$  and  $X_\infty := \text{Ric}(H_\infty) \geq 0$ .
- ii  $J_\infty \in \text{dom}(\text{Ric})$  and  $Y_\infty := \text{Ric}(J_\infty) \geq 0$ .
- iii  $\rho(X_\infty Y_\infty) < \gamma^2$ .

with  $\text{Ric}(H_\infty)$  being the Riccati operator,  $\rho$  being the spectral radius and  $\text{Ric}(H_\infty) \geq 0$  being an LMI, i.e., it refers to the real part of the eigenvalues of  $\text{Ric}(H_\infty)$ .

If the three conditions above are fulfilled, then the suboptimal controller is defined as

$$K_{sub} := \left[ \begin{array}{c|c} \hat{A}_\infty & -Z_\infty L_\infty \\ \hline F_\infty & 0 \end{array} \right] \quad (35)$$

where

$$\begin{aligned} \hat{A}_\infty &:= A + \gamma^{-2}B_1B_1^T X_\infty + B_2F_\infty + Z_\infty L_\infty C_2 \\ F_\infty &:= -B_2^T X_\infty \\ L_\infty &:= -Y_\infty C_2^T \\ Z_\infty &:= \left( I - \gamma^{-2}Y_\infty X_\infty \right)^{-1} \end{aligned}$$

In order to find an optimal controller, an iterative procedure in  $\gamma$  is implemented, searching for its minimum value. The implementation of this control strategy demonstrates efficient computation since the solution to the Riccati equations is constructed directly from the eigenvectors of both the  $H_\infty$  and  $J_\infty$  matrices. However, it must be noted that the proof of this algorithm does not ensure the internal stability of the controller. Remarkably, in the cases studied in this paper, the controller obtained is internally unstable, i.e., some poles of the controller are in the right half-plane. The stabilization of the controller is considered next.

#### 4.4. Strong Stabilization

As has been stated, one notable concern with the  $H_\infty$  approach is the fact that internal stability is not guaranteed [33]. The concept of internal stability remains crucial when implementing such controllers, as any deviation could lead to numerical errors and erratic controller behavior. Consequently, assuring the stability of an  $H_\infty$  design is imperative and demands independent verification.

The foundation of this control strategy rests on the distinct and unique stabilizing solution to the Riccati equations, resulting in what is commonly referred to as the “central controller”. Nevertheless, a family of admissible controllers that fulfill the condition  $\|T_{zw}\|_\infty < \gamma$  exists. Doyle [32] obtains them through the application of a linear fractional transformation (LFT [34]) between the central controller and an arbitrary matrix  $A_q$ . The central controller has the following form:

$$K_\infty(s) = \left[ \begin{array}{c|cc} A_c & B_{c1} & B_{c2} \\ \hline C_{c1} & D_{c11} & D_{c12} \\ C_{c2} & D_{c21} & D_{c22} \end{array} \right] = \left[ \begin{array}{c|cc} \hat{A}_\infty & -Z_\infty L_\infty & Z_\infty B_2 \\ \hline F_\infty & 0 & I \\ -C_2 & I & 0 \end{array} \right], \quad \|Q\|_\infty < \gamma \quad (36)$$

Based on this family of controllers, several authors have dealt with this problem. Campos-Delgado and Zhou [35] adopted an iterative approach to stabilize the original controller, creating a series of nested feedback loops. In this case, the main problem lies in the order of the resulting controller, since with each control loop, the order increases linearly. Most authors propose a solution based on coprime factorization [36,37].

Here, the approach proposed by Zeren and Özbay [38], which is built around the solution to two additional Algebraic Riccati Equations (AREs) will be applied.

For the existence of a stabilizing controller, the following conditions are necessary:

- i  $(A_c, B_{c2})$  is stabilizable and  $(C_{c2}, A_c)$  is detectable.
- ii  $A_c$  has no eigenvalues in the imaginary axis.

Provided these conditions are fulfilled, the stabilizing solution  $X$  to the following ARE is computed:

$$A_c^T X + X A_c - X B_{c2} B_{c2}^T X = 0, \quad X = X^T \geq 0 \quad (37)$$

Then, a stabilizing controller exists if a stabilizing solution exists for the ARE:

$$A_X Y + Y A_X^T - Y(\rho^2 C_{c2}^T C_{c2} - X B_{c2} B_{c2}^T X) Y + B_{c2} B_{c2}^T = 0, \quad Y = Y^T \geq 0 \quad (38)$$

with  $\rho$  being an arbitrary scalar and

$$A_X = A - B_{c2}B_{c2}^T X \quad , \quad F = -B_{c2}^T X$$

Under this sufficient condition,

$$K_q(s) = \left[ \begin{array}{c|c} A_q & B_q \\ \hline C_q & D_q \end{array} \right] = \left[ \begin{array}{c|c} A_K & -L \\ \hline F & 0 \end{array} \right] \tag{39}$$

is a strongly stabilizing controller with  $\|K\|_\infty \leq \rho$ , where

$$A_K = A_c + B_{c2}F + LC_{c2} \quad , \quad L = -\rho^2 Y C_{c2}^T$$

Since Equation (36) stated that the subcontroller must have an  $H_\infty$  norm under  $\gamma$ , then the calculation of the subcontroller  $K_q$  is an iterative procedure, starting with  $\rho = \gamma$ , with  $\rho$  being subsequently decreased so as to find an optimal subcontroller. In the case that for  $\rho = \gamma$  a solution to the aforementioned AREs cannot be reached, it can be concluded that a stabilizing controller does not exist.

With this additional feedback loop, the final state-space system of the controller corresponds to the linear fractional transformation  $K(s) = \text{LFT}(K_\infty, K_q)$ . Its state-space form is depicted as follows:

$$K(s) = \left[ \begin{array}{c|c} A_{K_\infty} & B_{K_\infty} \\ \hline C_{K_\infty} & 0 \end{array} \right] = \left[ \begin{array}{c|c} \left[ \begin{array}{cc} A_c & B_{c2}C_q \\ B_qC_{c2} & A_q \end{array} \right] & \left[ \begin{array}{c} B_{c1} \\ B_qD_{c21} \end{array} \right] \\ \hline [C_{c1} \quad D_{c12}C_q] & 0 \end{array} \right] \tag{40}$$

Following the same procedure as in the case of the compensator, the controller system is expressed as its transfer function form. This is required to be able to apply the p-method in the Laplace plane. The control law is then

$$u = C_{K_\infty}(sI - A_{K_\infty})^{-1}B_{K_\infty}y \tag{41}$$

Equations (27) and (28) are then used to obtain the dynamic equation of the system in a closed loop, substituting the compensator control law by the one presented here.

#### 4.5. Specific Control Law and Results

Once again for the parameters given in Table 1, the control procedure is tested on the airfoil in a compressible regime. Figure 7 shows the results. It can be seen that the branch corresponding to the plunging mode is stabilized before approaching the imaginary axis, averting any potential flutter issues. It is interesting to mention that after mitigating flutter, the system not only remains stable but also moves away from the imaginary axis.

In Figure 8, we present the system's pole distribution across the complete Laplace plane. A set of new branches emerged, positioned significantly distant from the imaginary axis, as in the previous case. Unlike the compensator scenario, the closed-loop poles in this case prove to be optimal and do not depend on arbitrary parameters.

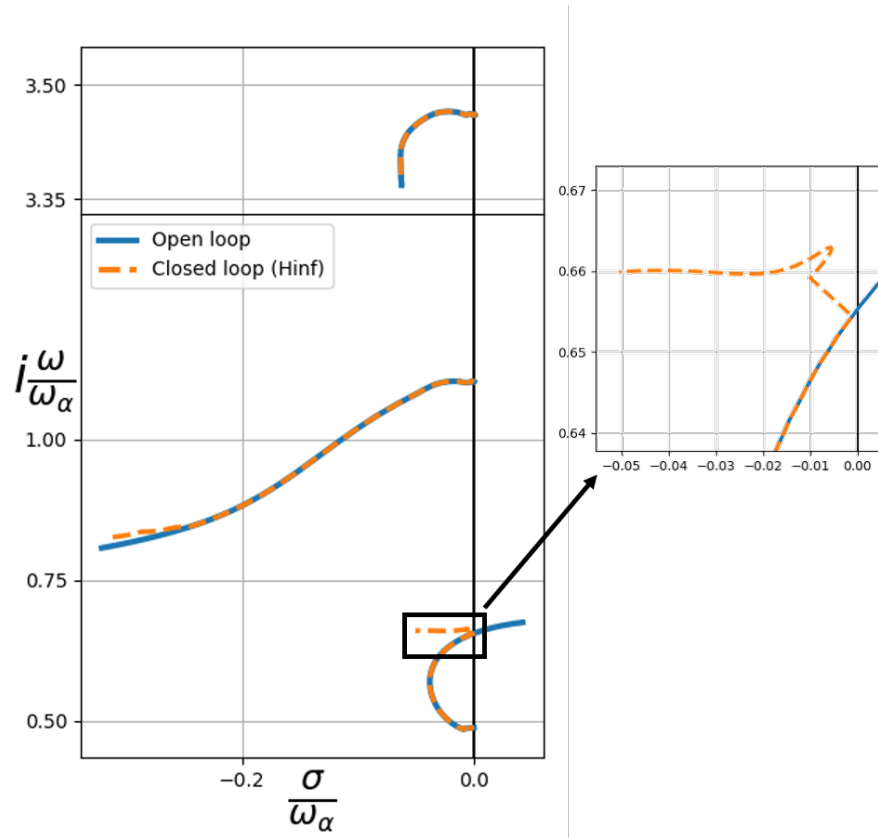


Figure 7. Root locus plot of a 3 dof airfoil in closed loop for  $M_\infty = 0.5$ . The control law was computed following the  $H_\infty$  approach.

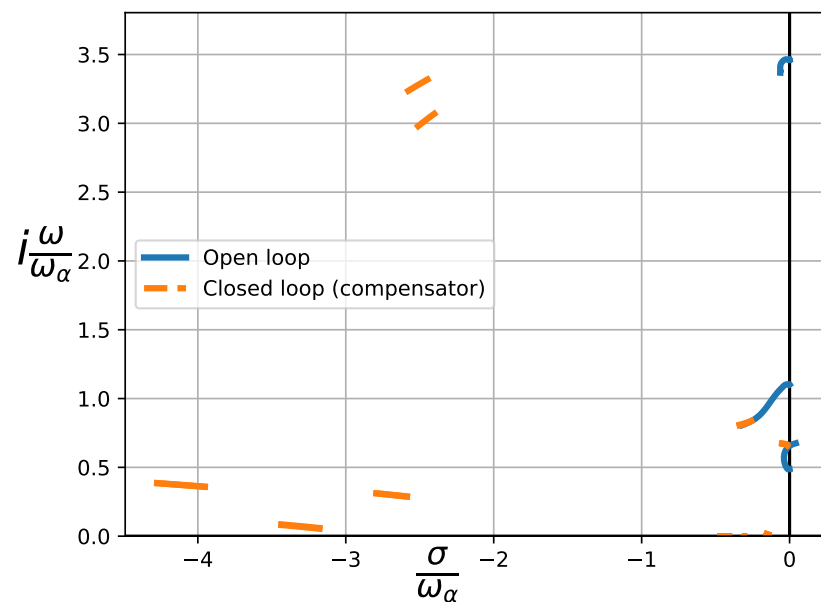
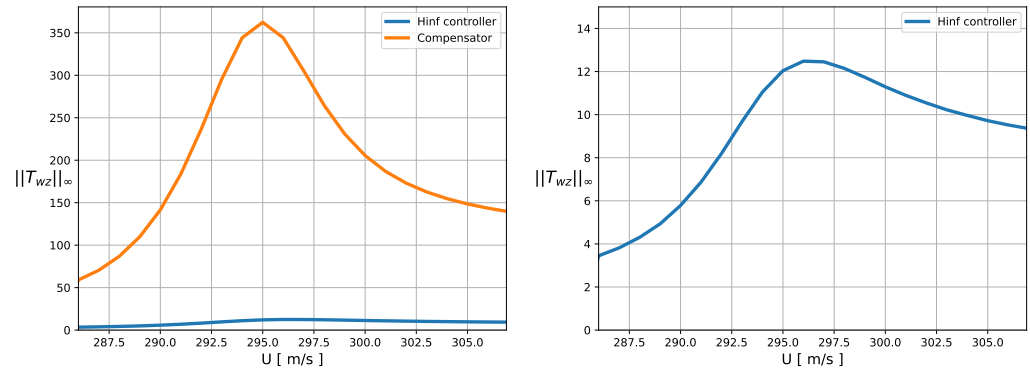


Figure 8. Root locus plot of the 3 dof airfoil with the  $H_\infty$  control law for  $M_\infty = 0.5$ , including new branches. These poles are associated with the controller dynamics.

### 5. Results for a Three Dof Airfoil

Following the results presented above for the closed-loop dynamics of the airfoil given in Table 1, a comparison of the two methods employed to obtain the control law is presented now. The effectiveness and efficiency of the system hinged upon the assessment of the  $H_\infty$  norm of the transfer function, specifically from exogenous inputs to regulated

outputs, is denoted as  $\|T_{zw}\|_\infty$ . It is essential to underscore that these regulated outputs encompass not only the system's states but also its inputs. Hence, a higher norm implies higher control effort from the actuator, which, in turn, may cause mechanical wear and tear on the system's actuators. Figure 9 shows this comparison. The  $H_\infty$  norm of the system in the case of the compensator is nearly two orders of magnitude higher than that of the  $H_\infty$  controller, thereby showing the efficiency of the  $H_\infty$  approach.



**Figure 9.** Evaluation of the  $\|T_{zw}\|_\infty$  norm: the closed-loop system for  $M_\infty = 0.5$ , comparing compensator and  $H_\infty$  controller efficiency.

With respect to the dynamics of the control law, Figure 10 shows the root locus of the two controllers. In both cases, the resulting controllers are stable, a prerequisite for the practicable deployment of the control loop, as previously highlighted. However, it is pertinent to acknowledge that the natural frequencies of the  $H_\infty$  poles are lower than the ones from the compensator. This implies that the  $H_\infty$  controller does not require internal dynamics as fast as the compensator, which is a positive point for its implementation (faster controllers are usually more expensive due to the necessity for high-speed processors and precision components to achieve rapid control responses).

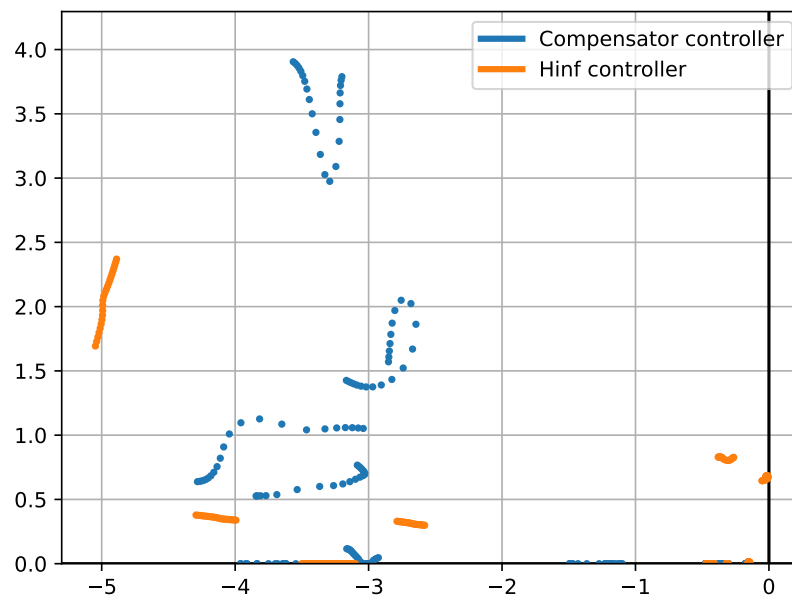
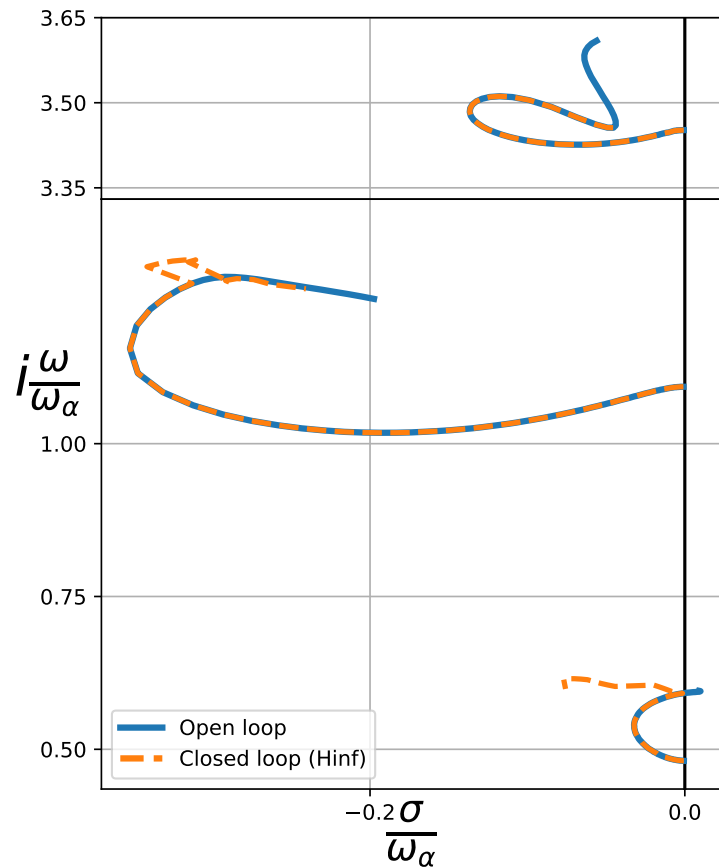


**Figure 10.** Comparison of the poles of the compensator and the  $H_\infty$  controller for  $M_\infty = 0.5$ .

Once the viability of this  $H_\infty$  implementation has been shown, it will be applied to a system in a compressible regime. It is important to highlight the fact that even though the control law was obtained by using a state-space modelization of the system, it is applied to

the exact dynamic equations and computed via the p-method. This ensures that the results will be as close to reality as possible.

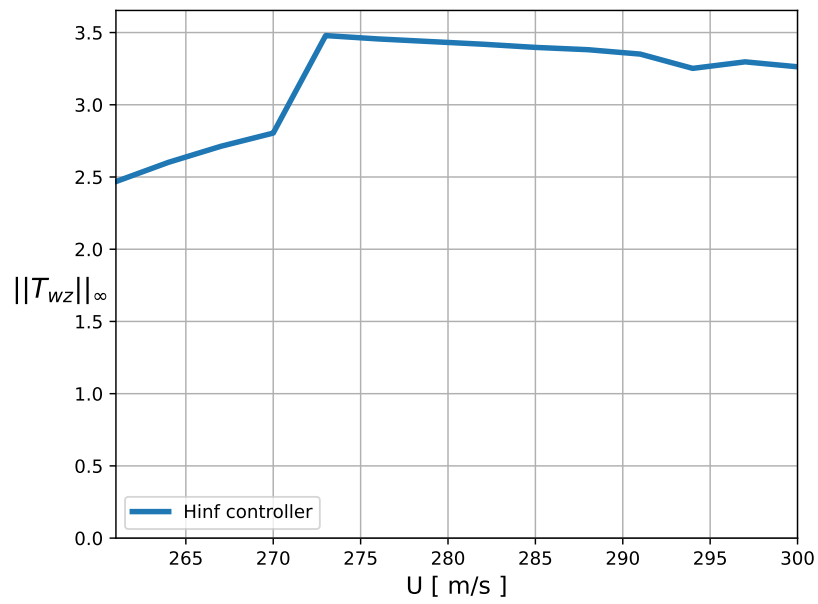
Figure 11 shows the root locus for the aforementioned airfoil, operating within subsonic, transonic and sonic regimes. Similar to the previous results, the controller is able to stabilize the system without any problem. In this case, we observe the influence of the controller on the torsion branch, even though it has little effect on its stability.



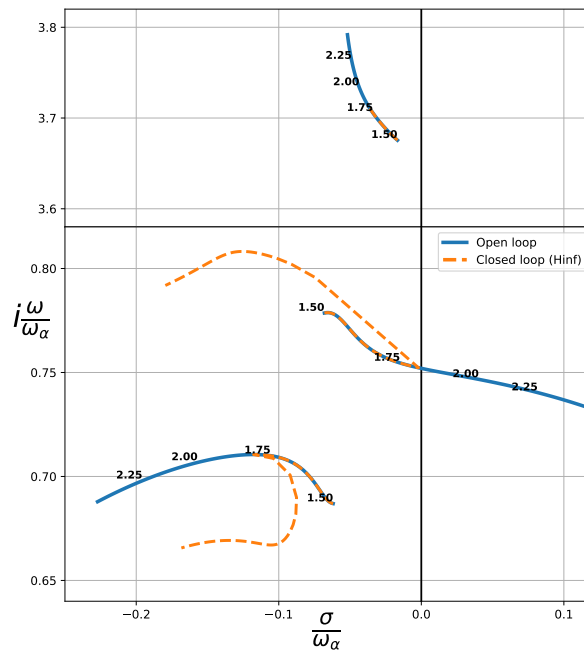
**Figure 11.** Root locus of a 3 dof airfoil in subsonic regime with an  $H_\infty$  controller. Mach numbers up to  $M_\infty = 1.0$  are considered, including transonic regime.

In the examination of the  $H_\infty$  norm for this closed-loop system, a noticeable dispersion in the results becomes apparent (Figure 12). This dispersion stems from the process of computing the state-space model for the airfoil, which involves determining the lags in Roger's RFA through an optimization procedure. These lags are inherently dependent on the Mach number. While the approximate model closely mimics the exact one, it is essential to acknowledge that numerical optimization is executed for each specific Mach number. Consequently, the obtained lags exhibit nonsmooth variations. One potential avenue to address this issue would involve the development of a regression model for the lags to ensure a smoother transition, though this solution requires further investigation to comprehensively consider all the contributing factors.

Next, to assess the method's suitability in a supersonic regime, we introduce a different airfoil configuration, characterized by the parameters delineated in Table 2. A sweep in the Mach number up to  $M_\infty = 2.5$  is performed, with  $a_\infty = 333$  m/s. The behavior of both the plunging and torsion modes is modified, as shown in Figure 13. Initially, the lower branch approaches the imaginary axis, subsequently reversing its direction. As the Mach number increases, all the modes seem to increase their stability. Regarding its performance, Figure 14 shows that the  $H_\infty$  controller performance also exceeds that of the compensator in this regime.



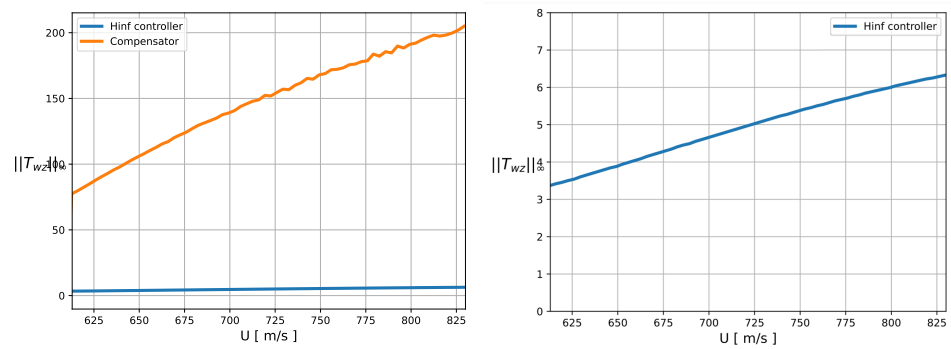
**Figure 12.** Evaluation of the  $\|T_{zw}\|_\infty$  norm for the closed-loop system in subsonic regime, comparing compensator and  $H_\infty$  controller efficiency.



**Figure 13.** Root locus of a 3 dof airfoil in supersonic regime with an  $H_\infty$  controller. Mach numbers up to 2.5 are considered.

**Table 2.** Three DOF section parameters for a wing section in supersonic flow, extracted from Table III-4 of Edward’s thesis [17].

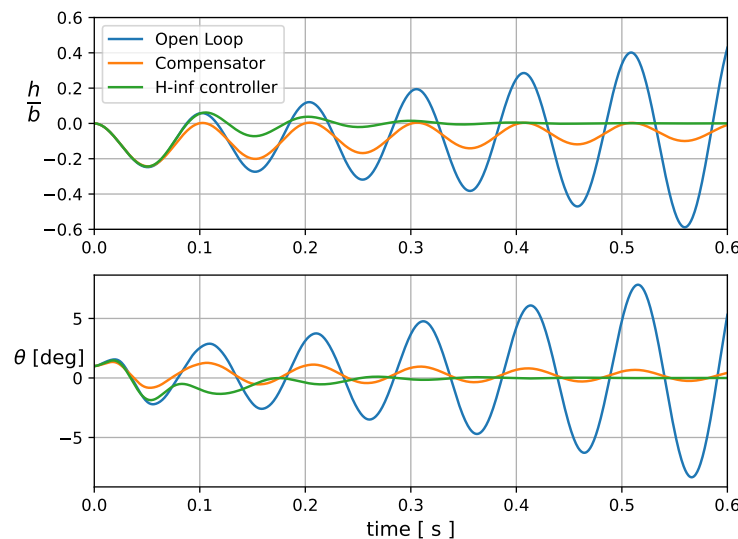
$\Lambda_1 = 0$	$\omega_h = 50 \text{ Hz}$	$x_\alpha = 0.2$	$x_\delta = 0.0125$
$b = 1.35$	$\omega_\alpha = 100 \text{ Hz}$	$r_\alpha^2 = 0.25$	$r_\delta^2 = 0.00625$
$\Lambda_3 = 0.6$	$\omega_\beta = 317 \text{ Hz}$	$\mu = 40$	$\zeta_\delta = 0$



**Figure 14.** Evaluation of the  $\|T_{zw}\|_{\infty}$  norm: the closed-loop system in supersonic regime, comparing compensator and  $H_{\infty}$  controller efficiency.

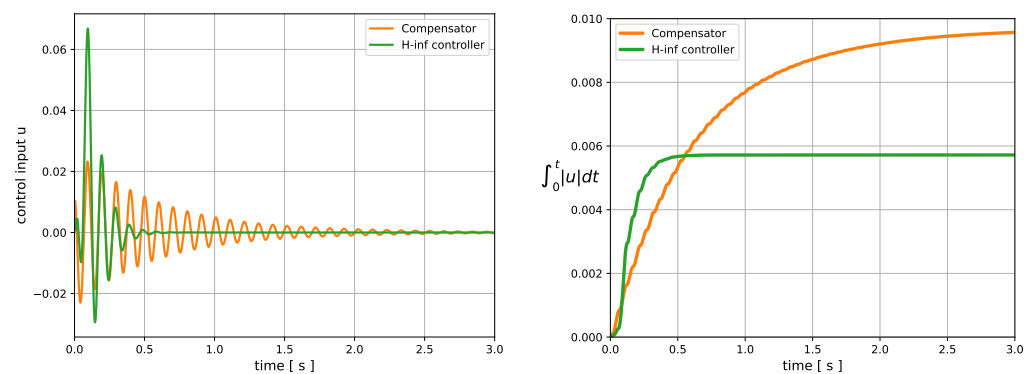
In order to exemplify the efficacy of the  $H_{\infty}$  method, we examine the behavior of the airfoil detailed in Table 1 in the time domain, specifically in the sonic regime with  $a_{\infty} = 340$  m/s. A numerical simulation is initiated with a minor perturbation in the torsional degree of freedom, and the equations are integrated by using the Crank–Nicolson method with a time step of 0.5 ms.

Figure 15 illustrates the evolution of the physical states of the airfoil. The open-loop system exhibits clear instability at this speed, surpassing the flutter velocity. As anticipated, upon closing the feedback loop, the system stabilizes and the oscillations of the states converge. Notably, the  $H_{\infty}$  controller demonstrates the faster damping of the oscillations compared to the compensator. To measure its performance, we introduce the settling time, defined as the duration for which oscillation amplitudes are confined within  $\pm 2\%$  of the initial perturbation. The compensator requires 2.85 s to settle, while the  $H_{\infty}$  controller achieves stabilization in just 0.47 s.



**Figure 15.** Time response of an inherently unstable airfoil in open and closed loop with nonzero initial conditions.

Regarding the control effort of the system, Figure 16 shows the input of the system resulting from the compensator and  $H_{\infty}$  controller, along with its integral over time, revealing the superior effectiveness of the  $H_{\infty}$  controller. Furthermore, the integral of the control input over time is lower in the case of  $H_{\infty}$ , suggesting reduced total energy consumption for stabilization. However, it is important to note that the maximum response required for control is higher with the  $H_{\infty}$  controller, a fact needed to be considered when implementing the control law in a real system.



**Figure 16.** Control input of an inherently unstable airfoil with nonzero initial conditions, stabilized with a compensator and an  $H_\infty$  controller.

## 6. Discussion

This report aimed to introduce a method for stabilizing aeroelastic systems that are inherently prone to flutter, a crucial issue in aeroelasticity. The control law is obtained based on unsteady aerodynamic force matrices that are valid in the full Laplace plane for the subsonic, sonic and supersonic flows. To assess the effectiveness of the proposed controller, we used the  $H_\infty$  norm, a standard measure of system robustness. To provide a performance baseline, we applied traditional control techniques, like pole placement and Linear Quadratic Regulator (LQR), to a three degree-of-freedom airfoil with a trailing-edge control surface.

Our chosen approach involved using an  $H_\infty$  controller, initially derived in a suboptimal closed form, which was later fine-tuned through an optimization process. We began by expressing the aeroelastic system through a linear relation with the  $s$  variable, transforming the system into a state-space representation, following a nine-matrix formulation. It is worth noting that the conventional  $H_\infty$  method does not guarantee internal controller stability. In response, a family of strongly stabilizing controllers, achieved by applying a linear fractional transformation (LFT) to the central controller, is introduced.

The distinctive contribution of this work lies in the practical application of the control law, seamlessly integrated into the exact dynamic equations (unsteady aerodynamics fully valid in the Laplace plane) of the aeroelastic system. Although the controller originated from a state-space model, it was later transformed into a transfer function in the Laplace domain and directly incorporated into the system's equations of motion. The p-method, a reliable analytical technique, to compute the system's poles across the three different branches corresponding to the physical modes, was used. This extensive analysis covered both subsonic and supersonic compressible flow regimes, resulting in the successful stabilization of the system. In all cases, the  $H_\infty$  norm outperformed the basic compensator.

Our research continues to progress, with ongoing investigations focused on extending this control methodology to aeroelastic wing systems. This represents a significant step in advancing the understanding and practical implementation of robust control strategies in the field of aeroelasticity. Currently, we are studying the application of this control system to a complete wing. Aerodynamic strip theory will be used, maintaining the theoretical basis presented here.

**Author Contributions:** Conceptualization, P.G.-F. and Á.M.; methodology, Á.M. and P.G.-F.; software, Á.M.; validation, Á.M.; formal analysis, Á.M.; investigation, Á.M. and P.G.-F.; resources, Á.M. and P.G.-F.; writing—review and editing, Á.M. and P.G.-F. All authors have read and agreed to the published version of the manuscript.

**Funding:** This research received no external funding.

**Data Availability Statement:** The original contributions presented in the study are included in the article, further inquiries can be directed to the corresponding author.

**Conflicts of Interest:** The authors declare no conflicts of interest.

## References

1. Pusch, M.; Ossmann, D.; Luspay, T. Structured Control Design for a Highly Flexible Flutter Demonstrator. *Aerospace* **2019**, *6*, 27. [CrossRef]
2. Edwards, J.W.; Ashley, H.; Breakwell, J.V. Unsteady Aerodynamic Modeling for Arbitrary Motions. *AIAA J.* **1979**, *17*, 365–374. [CrossRef]
3. Mordechay, K. Design for Active Flutter Suppression and Gust Alleviation Using State-Space Aeroelastic Modeling. *J. Aircr.* **1982**, *19*, 221–227.
4. Livne, E. Aircraft Active Flutter Suppression: State of the Art and Technology Maturation Needs. *J. Aircr.* **2018**, *55*, 410–449. [CrossRef]
5. Gangsaas, D.; Ly, U.L. Application of a Modified Linear Quadratic Gaussian Design to Active Control of a Transport Airplane. In Proceedings of the Guidance, Navigation and Control Conferences, Boulder, CO, USA, 6–8 August 1979.
6. Waszak, M.R. Robust Multivariable Flutter Suppression for Bench-mark Active Control Technology Wind-Tunnel Model. *J. Guid. Control. Dyn.* **2001**, *24*, 147–153. [CrossRef]
7. Zhao, Y.H. Flutter Suppression of a High Aspect-Ratio Wing with Multiple Control Surfaces. *J. Sound Vib.* **2009**, *324*, 490–513. [CrossRef]
8. Theis, J.; Pfifer, H.; Seiler, P.J. Robust Control Design for Active Flutter Suppression. In Proceedings of the AIAA SciTech Forum, Minneapolis, MN, USA, 4 January 2016.
9. Newsom, J.R.; Pototzky, A.S.; Abel, I. Design of a Flutter Suppression System for an Experimental Drone Aircraft. *J. Aircr.* **1985**, *22*, 380–386. [CrossRef]
10. Liebst, B.S.; Garrard, W.L.; Adams, W.M. Design of an Active Flutter Suppression System. *J. Guid. Control. Dyn.* **2001**, *19*, 64–71. [CrossRef]
11. Boyd, S.; Balakrishnan, V.; Kabamba, P. A bisection method for computing the  $H_\infty$  norm. *SIAM Rev.* **1990**, *32*, 318–334.
12. Chilali, M.; Gahinet, P.  $H_\infty$  design with pole placement constraints: An LMI approach. *IEEE Trans. Autom. Control.* **1996**, *41*, 358–367. [CrossRef]
13. Gahinet, P.; Apkarian, P. A linear matrix inequality approach to  $H_\infty$  control. *Int. J. Robust Nonlinear Control.* **1994**, *4*, 625–640. [CrossRef]
14. Darabseh, T.T.; Tarabulsi, A.M.; Mourad, A.-G.I. Active Flutter Suppression of a Two-Dimensional Wing using Linear Quadratic Gaussian Optimal Control. *Int. J. Struct. Stab. Dyn.* **2022**, *22*, 2250157. [CrossRef]
15. Micheli, B. Active Flutter Suppression of a Two-Dimensional Airfoil with Actuator Saturation. In Proceedings of the International Forum on Aeroelasticity and Structural Dynamics (IFASD), Madrid, Spain, 13–17 June 2022.
16. Muñoz, Á.; García-Fogeda, P. Active Flutter Suppression of a Wing Section in a Compressible Flow. *Aerospace* **2022**, *9*, 804. [CrossRef]
17. Edwards, J.W. Unsteady Aerodynamics Modelling and Active Aeroelastic Control. Ph.D. Thesis, SUDAAR 504, Stanford University, Stanford, CA, USA, 1977.
18. Karpel, M. Design for Active and Passive Flutter Suppression and Gust Alleviation. In NASA CR 3482; NASA: Washington, DC, USA, 1981.
19. Rott, N. Oscillating Airfoils at Mach Number 1. *J. Aeronaut. Sci.* **1949**, *16*, 380–381.
20. Roger, K.L. Airplane Math Modeling Methods for Active Control Design. *AGARD-CP-228* **1977**, 4.1–4.11.
21. Quero, D.; Vuillemin, P.; Poussot-Vassal, C. A generalized State-Space Aeroservoelastic Model Based on Tangential Interpolation. *Aerospace* **2019**, *6*, 9. [CrossRef]
22. Sherwood T.H.; Adams, W.M., Jr. Nonlinear Programming Extensions to Rational Function Approximation Methods for Unsteady Aerodynamic Forces. In *National Aeronautics and Space Administration; Scientific and Technical Information Division; NASA: Washington, DC, USA, 1988.*
23. Peters, D.A. Practical Applications of the Kalman Filter to Flutter Prediction and Control. *J. Guid. Control. Dyn.* **1991**, *14*, 531–537.
24. Caines, P. Review of ‘Linear Systems’ (Kailath, T.; 1980). *IEEE Trans. Inf. Theory* **1981**, *27*, 385–386. [CrossRef]
25. Nguyen, C.C. Arbitrary eigenvalue assignments for linear time-varying multivariable control systems. *Int. J. Control* **1987**, *45*, 1051–1057. [CrossRef]
26. Nguyen, C.; Lee, T.N. Design of a State Estimator for a Class of Time-Varying Multivariable Systems. *IEEE Trans. Autom. Control.* **1985**, *30*, 179–182. [CrossRef]
27. Valášek, M.; Olgac, N. Efficient Eigenvalue Assignments for General Linear MIMO Systems. *Automatica* **1995**, *31*, 1605–1617. [CrossRef]
28. Waitman, S.; Marcos, A.  $H_\infty$  Control Design for Active Flutter Suppression of Flexible-Wing Unmanned Aerial Vehicle Demonstrator. *J. Guid. Control.* **2019**, *43*, 656–672. [CrossRef]
29. Dantzig, G.B.; Orden, A.; Wolfe, P. Notes on Linear Programming: Part 1. The Generalized Simplex Method for Minimizing a Linear Form under Linear Inequality Restraints. 1954. Available online: <https://www.semanticscholar.org/paper/Notes-on-Linear-Programming%3A-Part-1.-The-Simplex-a-Dantzig-Orden/b35a57e72bf60e53bd31565679686d83e1a600fa> (accessed on 29 January 2024).
30. Helmsberg, C.; Rendl, F.; Vanderbei, R.J.; Wolkowicz, H. An Interior-Point Method for Semidefinite Programming. *SIAM J. Optim.* **1996**, *6*, 342–361. [CrossRef]

31. Scherer, C.W.; Gahinet, P.; Chilali, M. Multi-objective output-feedback control via LMI optimization. *IEEE Trans. Autom. Control.* **1997**, *42*, 896–911. [[CrossRef](#)]
32. Doyle, J.C.; Glover, K.; Khargonekar, P.P.; Francis, B.A. State-space solutions to standard  $H_2$  and  $H_\infty$  control problems. *IEEE Trans. Autom. Control.* **1989**, *34*, 831–847. [[CrossRef](#)]
33. Tewari, A. *Adaptive Aeroservoelastic Control*; Aerospace Series; Wiley: West Sussex, UK, 2015.
34. Packard, A.; Safonov, M. An overview of the linear-fractional transformation approach to control system analysis and synthesis. *Int. J. Control.* **1988**, *48*, 653–698.
35. Campos-Delgado, D.U.; Zhou, K.  $H_\infty$  strong stabilization. *IEEE Trans. Autom. Control.* **2001**, *46*, 1968–1972. [[CrossRef](#)]
36. Gumussoy, S.; Özbay, H. Remarks on strong stabilization and stable  $H_\infty$  controller design. *IEEE Trans. Autom. Control.* **2006**, *50*, 2083–2087. [[CrossRef](#)]
37. Zeren, M.; Özbay, H. On stable  $H_\infty$  controller design. *Proc. Am. Control. Conf.* **1997**, *2*, 1302–1306. [[CrossRef](#)]
38. Zeren, M.; Özbay, H. On the strong stabilization and stable  $H_\infty$ -controller design problems for MIMO systems. *Automatica* **2000**, *36*, 1675–1684. [[CrossRef](#)]

**Disclaimer/Publisher’s Note:** The statements, opinions and data contained in all publications are solely those of the individual author(s) and contributor(s) and not of MDPI and/or the editor(s). MDPI and/or the editor(s) disclaim responsibility for any injury to people or property resulting from any ideas, methods, instructions or products referred to in the content.